Journal of Cluster Science
https://doi.org/10.1007/s10876-024-02682-1

ORIGINAL PAPER

Fluorescent Nanoprobe Utilizing Tryptophan-Functionalized Silver Nanoclusters for Enhanced Gemcitabine Detection: Optimization and Application in Real Samples

Yahya S. Alqahtani[1] · Ashraf M. Mahmoud[1] · Al-Montaser Bellah H. Ali[2] · Mohamed M. El-Wekil[2]

Received: 10 April 2024 / Accepted: 31 July 2024

Abstract
A new "signal-off" probe based on silver nanoclusters modified with tryptophan amino acid (TRP@Ag NCs) has been developed for the sensitive and selective fluorometric detection of the anticancer drug gemcitabine. The probe exhibits a blue-emission at 460 nm upon excitation at 320 nm. Various reaction parameters were optimized to enhance the probe's performance. The addition of gemcitabine results in a decrease in the fluorescence emission, which is attributed to the aggregation of the TRP@Ag NCs. The interaction between the TRP@Ag NCs and gemcitabine involves multiple types of chemical bonds, including non-covalent hydrogen bonding, Van der Waals, and electrostatic forces. The fluorescence ratio (F°/F) exhibits a linear correlation with gemcitabine concentrations ranging from 0.005 to 60 µM, with a low limit of detection (LOD) of 1.7 nM (S/N=3). The TRP@Ag NCs probe demonstrates high sensitivity, good selectivity, and reliability. The developed probe was successfully applied for the detection of gemcitabine in authentic samples, including pharmaceutical injections, serum, and urine, with acceptable recovery percentages and low relative standard deviation (RSD), indicating the accuracy and reliability of the probe.

Keywords Gemcitabine · TRP@ Ag NCs · Aggregation-induced quenching · Electrostatic-interaction · Fluorescence

Introduction

The burgeoning growth of cancer research demands the creation of innovative analytical methodologies for accurately assessing chemotherapy medications [1]. It is imperative to prioritize the development of personalized treatment strategies that take into account individual patient responses and the unique characteristics of their disease [2]. This tailored approach aims to enhance treatment effectiveness while minimizing adverse effects. The successful execution of personalized medicine hinges on numerous factors, notably real-time patient health supervision through continuous monitoring of disease-related biomarkers and the amount of anti-cancer drugs in the bloodstream [3]. Administering micro-doses of drugs aims to attain optimal effects while minimizing adverse reactions. However, accurately detecting these drugs poses significant challenges, particularly when dealing with minimal concentrations in the bloodstream resulting from micro-dosing. This necessitates the utilization of highly sensitive detection techniques to ensure precise monitoring of drug levels. Gemcitabine, an anticancer medication, finds extensive application in treating various tumors including breast, ovarian, and pancreatic cancers [4]. Its mechanism involves DNA replication inhibition, favoring the tumor cell death [5]. Monitoring of gemcitabine levels in the bloodstream of patients is crucial due to its cytotoxic effects on normal cells [6]. Gemcitabine has been analytically determined using chromatographic [7–9] and electrochemical methods [10, 11]. While chromatographic techniques offer selectivity and sensitivity, they suffer from drawbacks such as complex instrumentation, the requirement for highly skilled personnel, extensive pretreatment steps, high costs, and time consumption [12, 13].

✉ Mohamed M. El-Wekil
mohamed.elwakeel@pharm.aun.edu.eg;
mohamed.mohamoud@ymail.com

[1] Department of Pharmaceutical Chemistry, College of Pharmacy, Najran University, Najran 11001, Saudi Arabia

[2] Department of Pharmaceutical Analytical Chemistry, Faculty of Pharmacy, Assiut University, Assiut 71516, Egypt

Published online: 25 August 2024

On the other hand, electrochemical methods lack selectivity due to electrode fouling [14, 15]. Hence, there is a critical need to develop simple, rapid, selective, and sensitive detection methods for gemcitabine in real samples. In contrast, optical methods, such as fluorometric techniques, emerge as relevant tools for measuring molecules and biomolecules due to their selectivity, rapidity, simplicity, sensitivity, and low-cost [16–21].

Metal nanoclusters are widely applied in the sensing area due to their excellent water dispersion, low toxicity, biocompatibility, stability, and photoluminescence properties [22–25]. Various fabrication methods, including electrochemical, chemical reduction, etching, microwave-assisted, and template approaches, are employed to produce metal nanoclusters [26–29]. Among the widely utilized nanoclusters are Cu NCs, Au NCs, and Ag NCs. Silver nanoclusters (Ag NCs) are preferred over gold and copper counterparts due to their lower cost compared to Au NCs and superior oxidation stability compared to Cu NCs [30, 31]. The stabilization of Ag NCs was achieved using various compounds such as bovine serum albumin [32], dihydrolipoic acid [33], and polyethyleneimine [34]. Among these, tryptophan (TRP) is particularly employed for stabilizing blue emissive nanoclusters due to its distinctive optical properties and inherent blue fluorescence after excitation in the range of 275–290 nm [35, 36]. Furthermore, when TRP is surface-modified onto nanoparticles, its fluorescence diminishes, thereby enhancing the exciton lifetime on the nanoparticles [37, 38]. In literature, tryptophan-functionalized silver nanoclusters (TRP@Ag NCs) were employed to determine Cu (II) [39] and Fe (III) [40].

Herein, we synthesized a new fluorescent probe comprising tryptophan-functionalized silver nanoclusters (TRP@Ag NCs) for detecting gemcitabine. The addition of cationic gemcitabine led to the quenching of negatively charged TRP@Ag NCs due to aggregation. This interaction between positively-charged gemcitabine and negatively-charged TRP@Ag NCs involves many types of interaction such as non-covalent hydrogen bonding, Van der Waals, and electrostatic force.

Experimental

Materials and Reagents

Gemcitabine (98.8%), Sodium borohydride ($NaBH_4$, 98.8%), dopamine (97.7%), ascorbic acid (96.8%), uric acid (98.3%), glutathione (97.9%), cysteine (98.6%), glucose (98.8%), glycine (97.5%), glutamine (98.7%), urea (97.6%), maltose (96.7%), and lysine (97.6%) were procured from Sigma Aldrich. Silver nitrate (99.8%), tryptophan (TRP, 97.8%), NaH_2PO_4, Na_2HPO_4, HCl, and NaOH were procured from Merck. GEMZAR® 200 mg injection was obtained from local markets.

Instruments and Quantum Yield (φ)

Description of instruments and calculation of φ (includes Fig. S1) were listed in supporting information.

Preparation of TRP@ Ag NCs

All glassware must underwent thorough rinsing with aqua regia (a mixture of HNO_3 and HCl, in a 1:3 v/v ratio) prior to being washed with ultrapure water. Subsequently, a solution consisting of 1.2 mL of 0.05 M $AgNO_3$, 1.8 mL of 0.5 M $NaBH_4$, and 1.5 mL of 0.05 M TRP was prepared, and the volume was adjusted to 8.0 mL using ultrapure water. The resulting mixture was stirred for 10 min at room temperature (RT). Following this, the pH of the mixture was adjusted to 5.0 before it was heated at 60 °C for 6 h. The resulting yellow-colored solution was then centrifuged at 3000 rpm for 20 min. The TRP@Ag NCs probe obtained in this manner was stored at 4 °C until further use (Scheme 1).

Determination of Gemcitabine

400 µL of the TRP@Ag NCs prepared earlier was combined with 600 µL of various concentrations of gemcitabine. The mixture was then allowed to incubate at RT for 2 min. After that, ultrapure water was used to complete the volume to 1.5 mL. Finally, the fluorescence spectra were then measured at 460 nm following excitation at 320 nm (Scheme 1).

Preparation of Samples

The injection sample was initially diluted with ultrapure water. Following this, 600 µL was combined with 400 µL of TRP@Ag NCs and allowed at RT for 2 min. Then, 1.5 mL of ultrapure water was added. For human serum and urine samples, they underwent centrifugation at 4000 rpm to eliminate suspended particles, after which they were diluted to 10 mL with ultrapure water. Next, 600 µL of the serum or urine was mixed with 400 µL of TRP@Ag NCs and incubated at RT for 2 min. Subsequently, 1.5 mL of ultrapure water was added. All samples were measured before and after addition of gemcitabine.

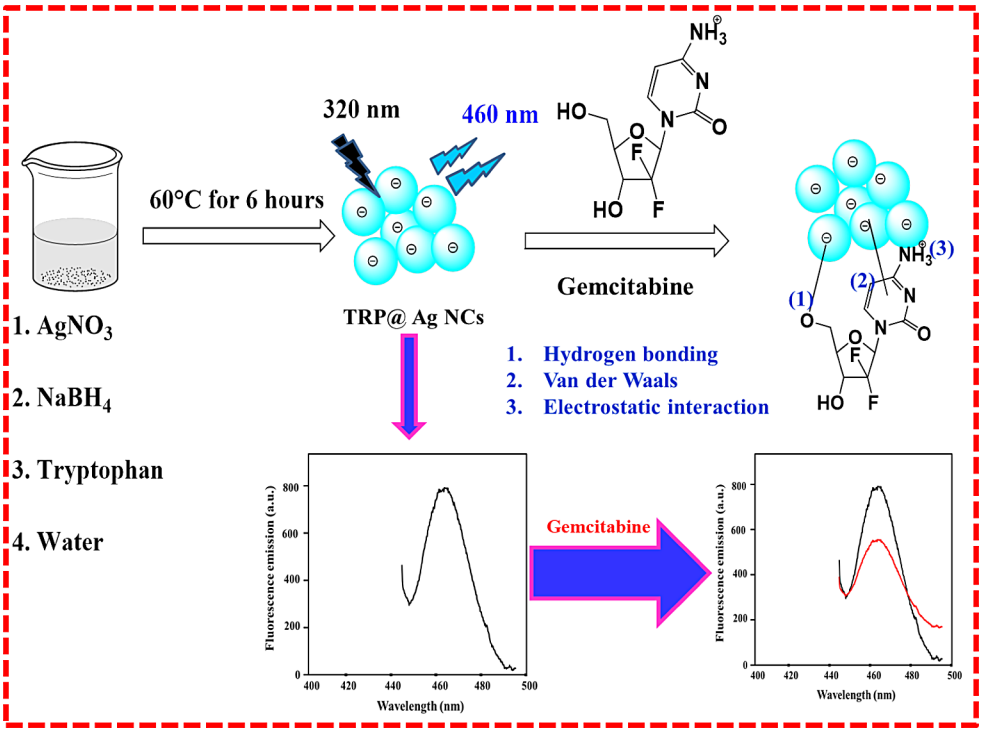

Scheme 1 Preparation of fluorescent TRP@ Ag NCs and determination of gemcitabine

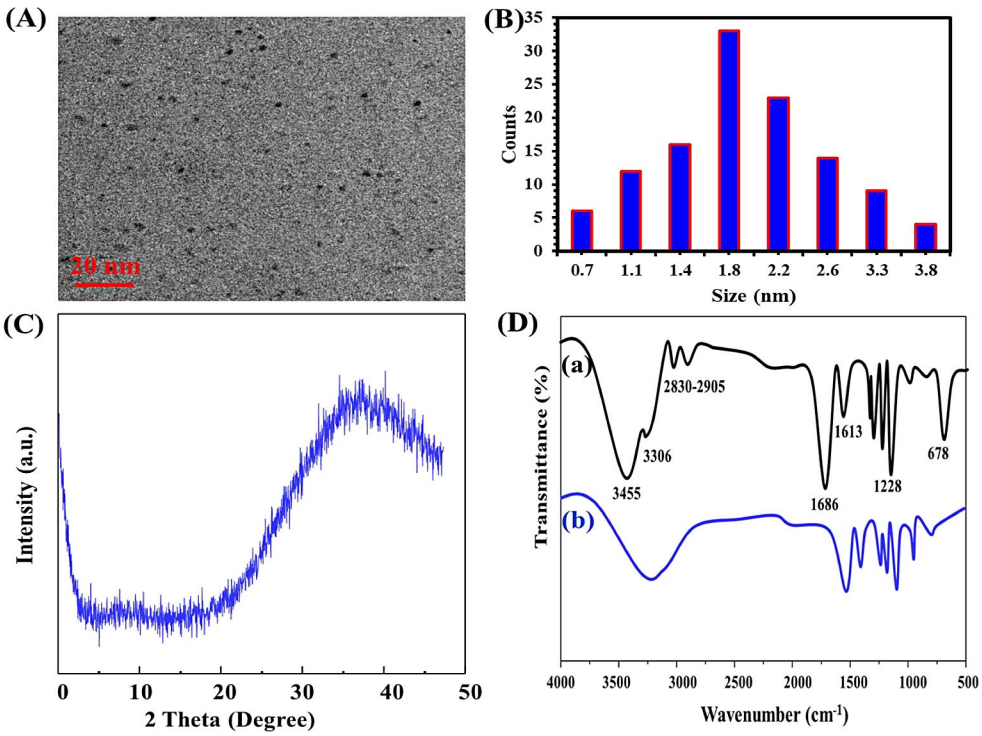

Fig. 1 TEM **(A)**, size distribution **(B)**, and XRD **(C)** of TRP@ Ag NCs while FT-IR spectra **(D)** of TRP (a) and TRP@ Ag NCs (b)

Results and Discussion

Characterization

The surface morphology of the probe was examined using TEM, as illustrated in Fig. 1A. The analysis revealed a spherical and well-dispersed pattern. Figure 1B presents the size distribution of the nanoclusters, indicating an average diameter of 1.8 nm ± 0.02 nm ($n = 80$). In Fig. 1C, the XRD pattern of the Ag NCs is depicted, with a diffraction peak observed at 38.9° and low intensity, indicating the formation of Ag NCs [41, 42]. Figure 1D showcases the modification of Ag NCs with TRP using FT-IR spectroscopy. In Fig. 1D(a),

the FT-IR spectrum of TRP displays main absorption bands at 3455 cm^{-1}, 3306 cm^{-1}, 1686 cm^{-1}, and 1228 cm^{-1}, corresponding to stretching vibrations of OH, NH, CH_2, C = O, and COO^-, respectively, while bands at 1613 cm^{-1} and 678 cm^{-1} represent bending vibrations of NH/OH and –NH-, respectively [43, 44]. Figure 1D(b) presents the FT-IR spectrum of TRP@Ag NCs, revealing a shift of fundamental bands to lower wavenumbers, which indicates successful modification of Ag NCs with TRP amino acid. Additionally, the absence of the bending vibration at 678 cm^{-1} confirms the chemical interaction between Ag NCs and TRP via –NH- functionality [45, 46]. Fig. S2A illustrates the binding energies of various elements, including C 1s, Ag 3d, N1s, and O 1s. It was observed that the binding energies for C 1s, Ag 3d, N1s, and O 1s were located at 293.6 eV, 369.8 eV, 398.7 eV, and 524.8 eV, respectively [47]. Fig. S2B presents the high-resolution XPS of Ag 3d, with binding energies at 368.5 eV and 371.7 eV, corresponding to Ag $3d_{5/2}$ and Ag $3d_{3/2}$, respectively [48]. These findings suggested that Ag (I) was successfully reduced to Ag (0) [49, 50].

In Figure 2A, the absorption spectrum of TRP@Ag NCs is depicted, showing peak absorption at 342 nm, potentially indicating the formation of nanoclusters [51]. The lack of surface Plasmon in the range from 400 nm to 500 nm confirms the formation of nanoclusters rather than nanoparticles [52]. Figure 2B presents the excitation/emission spectra of TRP@Ag NCs, with an emission wavelength of 460 nm observed following excitation at 320 nm. Figure 2C illustrates the relationship between emission wavelengths and excitation wavelengths. It was found that the emission wavelengths were red-shifted with increasing the excitation wavelengths, which may be attributed to the variation of size and/or surface functional groups on the surface of TRP@ Ag NCs [53]. Fig. S3 demonstrates the effect of hydrogen peroxide (H_2O_2) etching on the fluorescence response of TRP@Ag NCs. The addition of 10 µM H_2O_2 caused a slight decrease in the fluorescence emission of TRP@Ag NCs, which may be attributed to breaking down Ag NCs into Ag^+ [54].

To investigate the potential applications of TRP@ Ag NCs, we delved into their stability, as shown in Fig. S4. It was observed that the initially prepared probe displayed a remarkable level of stability even in high ionic strength conditions (Fig. S4a). Fig. S4b illustrates the exceptional stability of TRP@ Ag NCs across various pH values, which can be attributed to the protonation/deprotonation of surface functional groups. Notably, continuous irradiation of TRP@ Ag NCs for 150 min showed no discernible impact on the fluorescence readings of the probe, underscoring its robust stability (Fig. S4c). Furthermore, exposure of the probe to different temperatures (ranging from 25 to 45 °C) did not induce significant alterations in the fluorescence responses (Fig. S4d). The quantum photoluminescence yield was quantified at 9.78%.

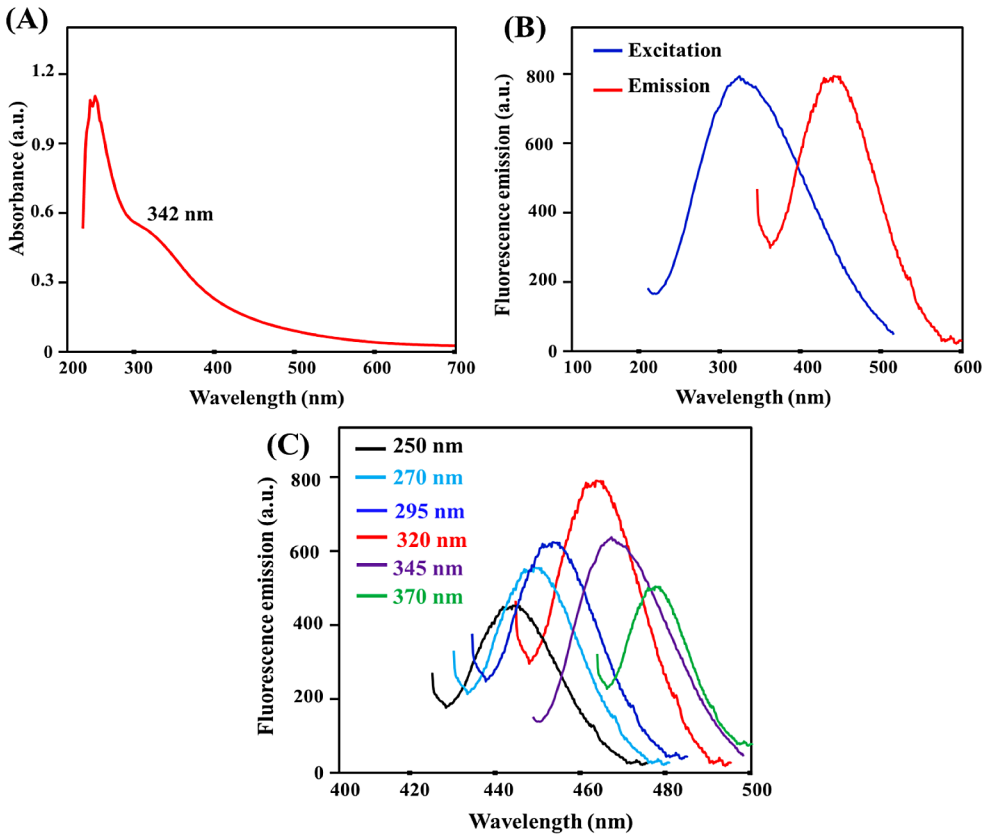

Fig. 2 Absorption spectra **(A)**, excitation/emission spectra **(B)**, and dependency of emission wavelength on the excitation wavelength of TRP@ Ag NCs **(C)**

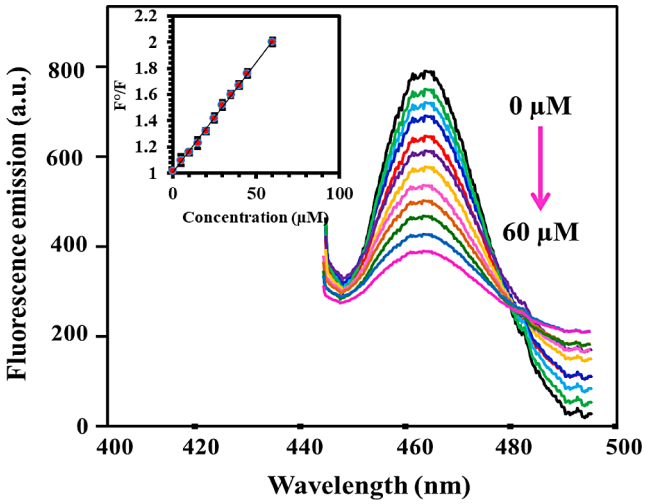

Fig. 3 The emission spectra of TRP@ Ag NCs diminish upon the addition of various amounts of gemcitabine (ranging from 0.005 to 60 µM) under optimal conditions. Inset displays the calibration plot. Diluting solvent used is water

Optimization of Detection Conditions

Factors influencing the interaction between TRP@Ag NCs and gemcitabine were carefully optimized. The effect of incubation time was investigated, revealing an optimal value of 2.0 min (Fig. S5a). Beyond this duration, the fluorescence reading stabilized, indicating saturation. Hence, 2.0 min was determined as the optimal incubation time for the interaction between TRP@Ag NCs and gemcitabine. Moreover, the pH value of the diluting solvent was explored using different solvents (Fig. S5b). It was observed that both H_2O and various buffers at pH 7.0 yielded similar outcomes. Consequently, H_2O was used as the diluting solvent for the entire study, ensuring consistency in the experimental conditions. Additionally, the effect of different pH values was tested using phosphate buffer in the range of 5.0 to 9.0 (Fig. S5c). The results indicated that pH 7.0 provided the best response. Therefore, pH 7.0 was selected as the optimal pH for subsequent determinations. Fig. S5d shows the effect of TRP@Ag NCs amounts on the sensing of gemcitabine. It was evident that 400 µL of TRP@Ag NCs was the optimal amount. Below this value, the fluorescence ratio remained constant.

Detection of Gemcitabine Using TRP@ Ag NCs

The newly developed fluorescent probe was utilized to assess various concentrations of gemcitabine under optimal conditions. Figure 3 illustrates the decrease in fluorescence responses of TRP@ Ag NCs upon addition of gemcitabine within the range of 0.005-60 µM, attributable to aggregation-induced quenching. The plot depicting the relationship between the fluorescence ratio (F°/F, where F and F° represent fluorescence readings after and before gemcitabine addition, respectively) and gemcitabine concentration demonstrates a linear correlation with a high determination coefficient (R^2) of 0.9982 and a regression equation of $F°/F = 1.005 + 0.0167\ C_{\text{gemcitabine}}$. The limit of detection (LOD) was calculated based on signal to noise = 3:1 and calculated as 1.7 nM. Comparative analysis of the analytical parameters between the proposed probe and other methods detailed in the literature for gemcitabine determination is presented in Table 1. It was concluded that the TRP@ Ag NCs probe exhibits the lowest LOD and a wide-dynamic linear range for the drug determination.

Table 1 Different analytical methods for the determination of gemcitabine

Methods	Dynamic linear range (µM)	LOD (µM)	Reference
Spectrophotometry	5.1- 151.9	1.67	[55]
	0.57–56.9	0.46	[56]
HPLC/UV	0.49–56.9	0.34	[56]
Electrochemical	0.1–150	0.011	[10]
	0.01–30	0.005	[11]
	0.1–15	0.05	[57]
	3.5-113.9	1.04	[58]
Fluorometric methods	0.003–0.1	0.002	[59]
	0.3–100	0.1	[60]
	0.005-60	0.0017	**This work**

Anti-interference Study

The study investigated the impact of common interfering species on the fluorescence readings of TRP@Ag NCs (Fig. 4). It was found that 600 µM of Na^+, K^+, Ca^{2+}, Mg^{2+}, Cl^-, CO_3^{2-}, and PO_4^{3-}; 500 µM of ascorbic acid, dopamine, uric acid, and glycine; 350 µM of urea, glucose, and maltose; and 300 µM of glutathione, cysteine, and glutamine did not significantly influence the fluorescence signal of the fluorescent probe. Moreover, the selectivity of the proposed probe was investigated in the presence of co-administered anti-cancer drugs used with gemcitabine. It was found that 300 µM anti-cancer drugs including, cisplatin, oxaliplatin, carboplatin, 5-fluorouracil, and imatinib did not remarkably affect the fluorescence response of the probe. These results suggest the probe has good selectivity.

Applications

The newly prepared TRP@AgNCs fluorescent probe was employed for the estimation of gemcitabine in various real samples, including injections, serum, and urine. The standard addition method was utilized to quantify the drug in these matrices. Table 2 illustrates that the recovery

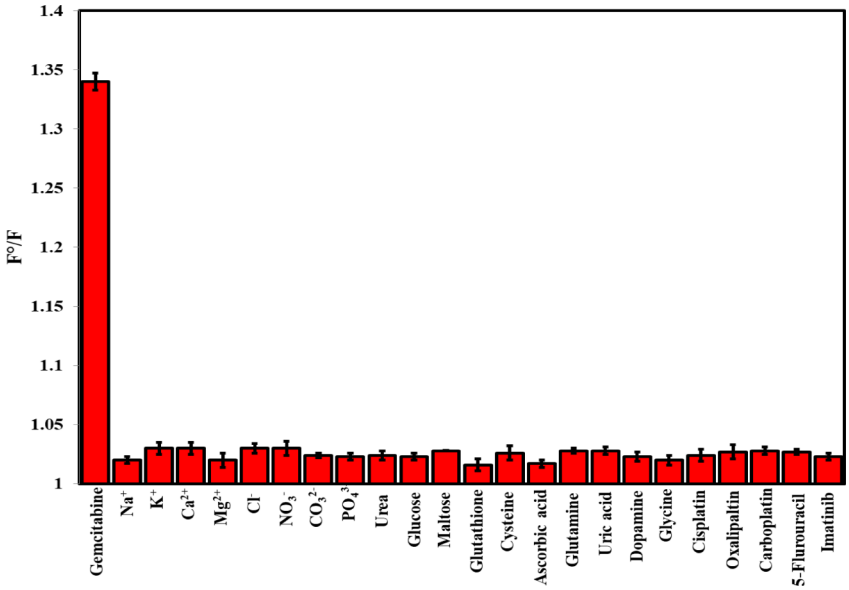

Fig. 4 The selectivity of the proposed TRP@Ag NCs fluorescent probe for detection of gemcitabine

Table 2 Determination of gemcitabine in real samples (n=5)

Sample	Added (µM)	Proposed method			Reported HPLC/UV method [61]		
		Found (µM)	Recovery %	RSD %	Found (µM)	Recovery %	RSD %
Injection	0.0	4.98	------	------	4.89	------	------
	0.01	5.02	100.6	3.45	4.86	97.4	3.78
	1.0	5.93	99.1	2.67	6.15	104.4	4.34
	5.0	10.04	100.6	3.78	10.34	104.6	4.78
Serum	0.0	------	------	------	------	------	------
	1.0	1.02	102.0	2.98	1.05	105.0	3.65
	5.0	4.97	99.4	3.34	5.04	100.8	4.09
	10.0	10.03	100.3	3.87	9.64	96.4	4.78
Urine	0.0	------	------	------	------	------	------
	1.0	0.97	97.0	3.26	1.04	104.0	3.45
	5.0	4.97	99.4	3.34	5.08	101.6	4.23
	10.0	10.01	100.1	2.89	10.56	105.6	4.65

percentages ranged between 97.0% and 102.0%, with RSD% falling within the range of 2.67–3.87%. Moreover, the results of the fluorescent probe were compared with a standard HPLC/UV method [61] for determining gemcitabine in real samples. These findings demonstrate the robustness and reliability of the method for detecting gemcitabine in these matrices.

Mechanism

The fluorescence feature at the surface of nanoclusters/nanoparticles is closely linked to physical or chemical changes that occur during their interactions [62, 63]. Spectroscopic and microscopic analyses were conducted to elucidate the detection mechanism between TRP@Ag NCs and gemcitabine (Fig. 5). The lack of overlap between the UV/Vis of gemcitabine and the emission spectrum of TRP@Ag NCs eliminates the possibility of Förster resonance energy transfer (FRET) or inner-filter effect (IFE), as depicted in Fig. 5a. TEM imaging was performed after introducing gemcitabine (Fig. 5b), revealing aggregation and an increase in the particle size of nanoclusters, consequently leading to a reduction in fluorescence [64]. Dynamic light scattering (DLS) measurements were taken before and after introducing gemcitabine. The DLS of TRP@Ag NCs was found to be 108.5 ± 5.67 nm (Fig. 5c), whereas that of TRP@Ag NCs/gemcitabine was 248.8 ± 8.32 nm (Fig. 5d), confirming the aggregation of nanoclusters following the introduction of the drug, consistent with TEM observations. The zeta potentials of TRP@Ag NCs and TRP@Ag NCs/gemcitabine were measured as -32.45 mV and − 8.78 mV, respectively (Fig. 5e). Reduction in the surface negative charge of the initially prepared TRP@Ag NCs after the addition of gemcitabine can be attributed to the cationic nature of the drug, which diminishes the surface charge of the negative-charged nanoclusters. Figure 5f illustrates the fluorescence lifetimes of TRP@Ag NCs and TRP@Ag NCs/gemcitabine, which remained unchanged, indicating static quenching [65]. Figure 6A illustrates the

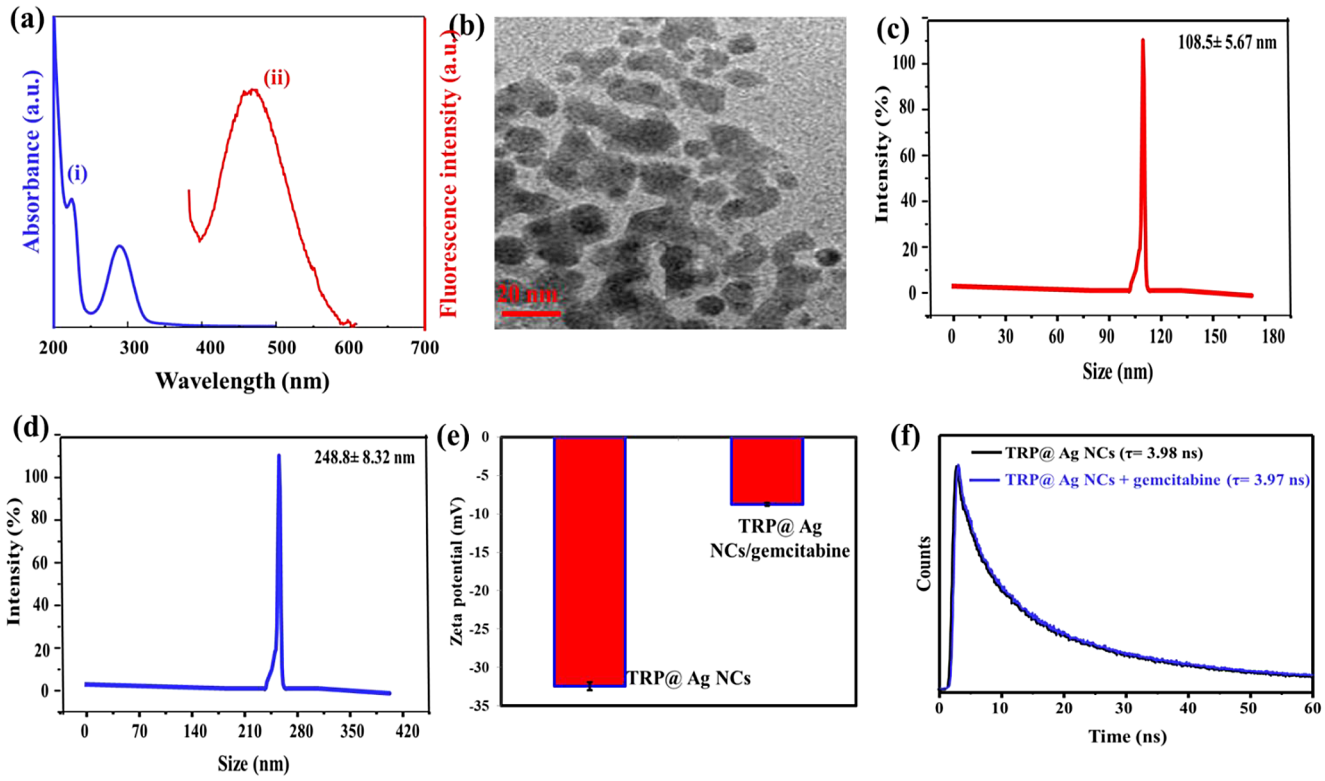

Fig. 5 **(a)** UV/Vis absorption spectrum of gemcitabine (i) and fluorescence emission spectrum of TRP@ Ag NCs (ii); **(b)** TEM image of TRP@ Ag NCs after addition of gemcitabine; **(c)** DLS of TRP@ Ag NCs; **(d)** DLS of TRP@ Ag NCs after addition of gemcitabine; **(e)** Zeta potentials of TRP@ Ag NCs and TRP@ Ag NCs /gemcitabine : **(f)** Fluorescence life times of TRP@ Ag NCs in absence and presence of 100 µM gemcitabine

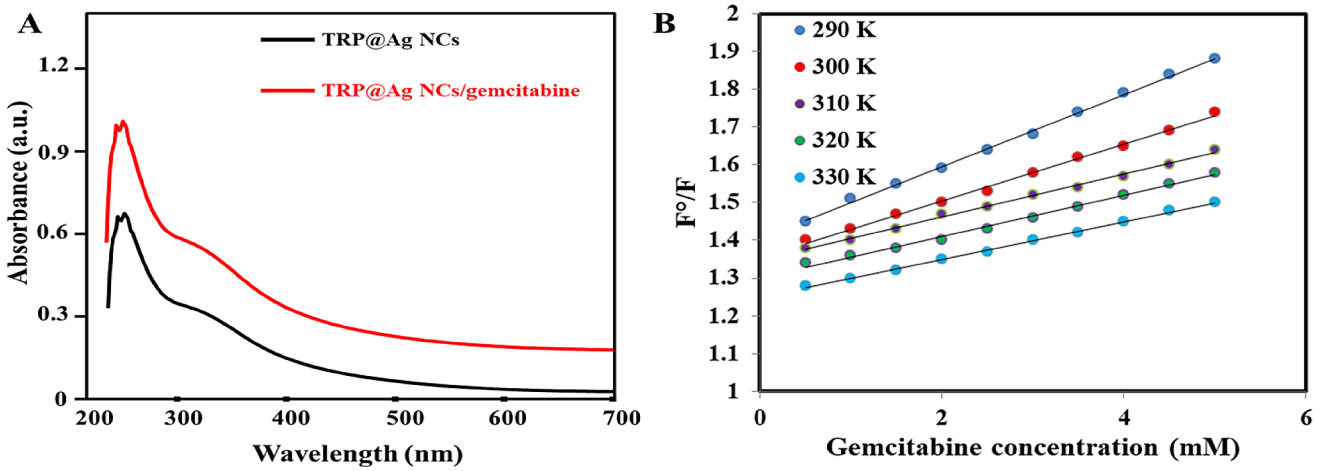

Fig. 6 **(A)** The UV/Vis absorption spectra of TRP@ Ag NCs and TRP@ Ag NCs/ gemcitabine. **(B)** Stern-Volmer calibration plots at 290 K, 300 K, 310 K, 320 K, and 330 K

effect of gemcitabine addition on the UV/Vis spectrum of TRP@Ag NCs. The addition of gemcitabine increases the absorption intensity of the nanoclusters, suggesting the static quenching between gemcitabine and TRP@Ag NCs. Figure 6B shows the Stern-Volmer plots for TRP@ Ag NCs with varying concentrations of gemcitabine. The data indicate that the slope (Ksv) increases with rising temperature, suggesting static quenching [66, 67].

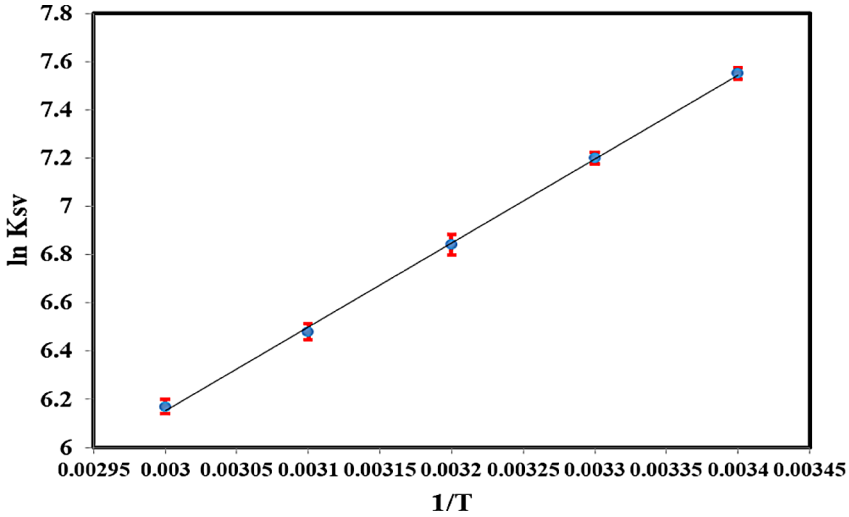

Fig. 7 Plot relationship between Ksv and 1/T

Binding Energies Analysis

Thermodynamic parameters, were estimated using the following equation to understand the nature of interactions between gemcitabine and TRP@Ag NCs:

$$ln\,Kb = -\frac{\Delta H}{RT} + \frac{\Delta S}{R}$$

Here, Kb equals the Stern-Volmer constant (Ksv) and R is the universal gas constant [68]. By plotting the relationship between lnKb and 1/T (Fig. 7), the values of ΔH and ΔS can be obtained. The change in free energy (ΔG) can be calculated using the following equation:

$$\Delta G\ (T) = \Delta H - T\Delta S$$

The models of interaction between gemcitabine and TRP@Ag NCs can be categorized as follows: (i) if both ΔS and ΔH are positive, it suggests hydrophobic interactions. (ii) if both ΔS and ΔH are negative, it indicates hydrogen bonding and Van der Waals forces. (iii) if ΔS is positive and ΔH is negative, it suggests electrostatic interactions [69, 70]. Table S1 shows that both ΔS and ΔH are negative, indicating that the main interactions between gemcitabine and TRP@Ag NCs are hydrogen bonding, Van der Waals forces, and electrostatic interactions. Additionally, the negative sign of ΔG indicates that the interaction between them is spontaneous.

Conclusions

A novel blue-emitting "signal-off" probe comprising tryptophan-functionalized silver nanoclusters (TRP@Ag NCs) was synthesized to detect gemcitabine. Upon exposure to gemcitabine, the TRP@Ag NCs probe experienced quenching due to aggregation, facilitated by hydrogen bonding, π-π stacking, and electrostatic attraction. Optimization of factors influencing the detection sensitivity was conducted. The fluorescent probe demonstrated notable selectivity, rendering it suitable for practical applications. Successful application of the TRP@Ag NCs probe was demonstrated in detecting gemcitabine in pharmaceutical injections, human serum, and urine samples.

Supplementary Information The online version contains supplementary material available at https://doi.org/10.1007/s10876-024-02682-1.

Acknowledgements The authors are thankful to the Deanship of Graduate Studies and Scientific Research at Najran University for funding this work under the Growth Funding Program grant code (NU/GP/MRC/13/237-1).

Author Contributions Yahya S. Alqahtani, Ashraf M. Mahmoud, Mohamed El-Wekil: Conceptualization, Data Curating, Formal Reviewing and Analysis; Ramadan Ali: Writing, Editing, Reviewing and Supervision.

Data Availability No datasets were generated or analysed during the current study.

Declarations

Ethical Approval The research followed the guidelines set forth by the Egyptian authorities and obtained approval from the Institutional Human Ethics Committee at Assiut University, Egypt.

Competing Interests The authors declare no competing interests.

References

1. Y. Pashaei, M. Mehrabi, M. Shekarchi, A review on various analytical methods for determination of anthracyclines and their

metabolites as anti–cancer chemotherapy drugs in different matrices over the last four decades. TrAC, Trends Anal. Chem., 130 (2020), Article 115991.
2. A. Hoeben, E.A. Joosten, M.H. van den Beuken-van Everdingen, Personalized medicine: recent progress in cancer therapy. Cancers, 13 (2) (2021), p. 242.
3. C.W. Chan, B.M. Law, W.K. So, K.M. Chow, M.M. Waye, Novel strategies on personalized medicine for breast cancer treatment: an update. Int. J. Mol. Sci., 18 (11) (2017), p. 2423.
4. I. Rus, A. Pusta, M. Tertiș, C. Barbălată, I. Tomuță, R. Săndulescu, C. Cristea, Gemcitabine direct electrochemical detection from pharmaceutical formulations using a boron-doped diamond electrode. Pharmaceuticals, 14 (9) (2021), p. 912.
5. L. de Sousa Cavalcante, G. Monteiro, Gemcitabine: metabolism and molecular mechanisms of action, sensitivity and chemoresistance in pancreatic cancer. Eur. J. Pharmacol., 741 (2014), pp. 8–16.
6. M. Garcia-Gil, B. Turri, M. Gabriele, L. Pucci, A. Agnarelli, M. Lai, G. Freer, M. Pistello, R. Vignali, R. Batistoni, Protopine/gemcitabine combination induces cytotoxic or cytoprotective effects in cell type-specific and dose-dependent manner on human cancer and normal cells. Pharmaceuticals, 14 (2) (2021), p. 90.
7. M. M. Z. Sharkawi, N. R. Mohamed, M. T. El-Saadi, N. H. Amin, FDA-Validated Ecofriendly Chromatographic Methods for Simultaneous Determination of Gemcitabine and Sorafenib: Applications to Pharmacokinetics. Chromatographia 86 (2023), pp. 109–123.
8. M. Wang, R. Hiraki, N. Nakamura, T. Hayama, T. Yasuda, Y. Miyata, H. Sakai, M. N. Nakashima, M. Nakashima, K. Ohyama, Determination of Gemcitabine in Plasma of Bladder Cancer Patients by Hydrophilic Interaction Chromatography with Ultraviolet Detection. J. Chromatographic Science 58 (2020), pp. 587–590.
9. H. Khoury, A. Deroussent, L. H. Reddy, P. Couvreur, G. Vassal, A. Paci, Simultaneous determination of gemcitabine and gemcitabine-squalene by liquid chromatography–tandem mass spectrometry in human plasma. J. Chromatogr. B 858 (2007), pp. 71–78.
10. B. Hatamluyi, S. Sadeghzadeh, R. Sadeghian, M. M. Mirimoghaddam, M. T. Boroushaki, A signal on-off ratiometric electrochemical sensing platform coupled with a molecularly imprinted polymer and $CuCo_2O_4$/NCNTs signal amplification for selective determination of gemcitabine. Sens. Actuat. B: Chem. 371 (2022), Article 132552.
11. H. Karimi-Maleh, N. Erk, Gemcitabine drug intercalation with ds-DNA at surface of ds-DNA/Pt–ZnO/SWCNTs/GCE biosensor: A DNA-biosensor for gemcitabine monitoring confirmed by molecular docking study. Chemosphere 336 (2023), Article 139268.
12. M. H. Mahnashi, A. M. Mahmoud, K. Alhazzani, A.Z. Alanazi, M. M. Algahtani, A. M. Alaseem, Y. S.A. Alqahtani, M. M. El-Wekil, Enhanced molecular imprinted electrochemical sensing of histamine based on signal reporting nanohybrid. Microchem. J. 168 (2021), Article 106439.
13. A. M. Mahmoud, S. A. Alkahtani, B. A. Alyami, M. M. El-Wekil, Dual-recognition molecularly imprinted aptasensor based on gold nanoparticles decorated carboxylated carbon nanotubes for highly selective and sensitive determination of histamine in different matrices. Anal. Chem. Acta 1133 (2020), pp. 58–65.
14. A.M. Mahmoud, M.H. Mahnashi, A. Al Fatease, M.A.H. Mostafa, M.M. El-Wekil, R. Ali, Fluorometric and electrochemical dual-mode detection of toxic flavonoid rutin based on new nitrogen and sulfur co-doped carbon dots: Enhanced selectivity based on masking the interfering flavonoids with BSA complexation, Journal of Food Composition and Analysis, 108 (2022) 104428.
15. R. M.K. Mohamed, S. H. Mohamed, A. M. Asran, I. H. Alsohaimi, H. M.A. Hassan, H. Ibrahim, M. M. El-Wekil. Bifunctional ratiometric sensor based on highly fluorescent nitrogen and sulfur biomass-derived carbon nanodots fabricated from manufactured dairy product as a precursor. Spectrochimica Acta Part A: Molecular and Biomolecular Spectroscopy 293 (2023), Article 122444.
16. S. Swathy, S.K. Anand, M.R. Mathew, K. Girish Kumar, Thioglycolic acid capped cadmium sulphide quantum dots as a turn-on fluorescence sensor for the determination of 5-hydroxyindoleacetic acid. J. Photochem. Photobiol. Chem., 409 (2021), Article 113145.
17. A.M. Mahmoud, M.H. Mahnashi, F.M. Alshareef, M.M. El-Wekil, Functionalized vanadium disulfide quantum dots as a novel dual-mode sensor for ultrasensitive and highly selective determination of rutin, Microchemical Journal, 187 (2023) 108430.
18. K. Sasikumar, R. Rajamanikandan, H. Ju, Fluorescent carbon dots for highly sensitive bilirubin sensing with excellent selectivity. J. Sci. Adv. Mat. Dev. 8 (2023), p. 100599.
19. R. Rajamanikandan, M. Ilanchelian, H. Ju, Highly selective uricase-based quantification of uric acid using hydrogen peroxide sensitive poly-(vinylpyrrolidone) templated copper nanoclusters as a fluorescence probe. Chemosensors 11 (2023), p. 268.
20. U. Subramani, R. Rajamanikandan, K. S. Mani, Coumarin hemicyanine-based colorimetric, smartphone color ratio, and intramolecular charge transfer fluorescent receptor for highly specific sensing of hydrazine in environmental water samples. J. Mol. Liq. 385 (2023), p. 122442.
21. A.M. Mahmoud, M. M. El-Wekil, R. Ali, H. A Batakoushy, R. Y. Shahin, Double-signal quantification of amoxicillin based on interaction with 4-aminoantipyrine at copper and nitrogen co-doped carbon quantum dots as an artificial nanozyme. Microchem. Acta 189 (2022), p. 183.
22. Q.F. Zhuang, C. Zeng, Y.X. Mu, T. Zhang, G.T. Yi, Y. Wang, Lead(II)-triggered aggregation-induced emission enhancement of adenosine-stabilized gold nanoclusters for enhancing photoluminescence detection of nabam-disodium ethylenebis(dithiocarbamate). Chem. Eng. J., 470 (2023), Article 144113.
23. A.M. Mahmoud, M.H. Mahnashi, M.M. El-Wekil, Ratiometric fluorescence sensing of hazardous ciprofloxacin based on aggregation induced emission enhancement of thiolate-protected gold nanoclusters induced by La^{3+} ion. Spectrochim. Acta Part A: Mol. Biomol. Spectr. 304 (2024), Article 123347.
24. B.A. Alyami, A.M. Mahmoud, A.O. Alqarni, A.B.H. Ali, M. El-Wekil, Ratiometric fluorometric determination of sulfide using graphene quantum dots and self-assembled thiolate-capped gold nanoclusters triggered by aluminum. Microchim. Acta, 190 (2023) 467.
25. .S. Bahota, K.K. Singh, A. Yadav, R. Chaudhary, N. Agrawal, P. Tandon, First principal study of interaction of copper doped gold nanoclusters with glycine. Inorg. Chem. Commun., 151 (2023), Article 110435.
26. T.R. Zou, S.Q. Li, G.X. Yao, R. Qu, W.R. Yang, H.B. Wang, W. Tan, M. Yang, Highly photoluminescent tryptophan-coated copper nanoclusters based turn-off fluorescent probe for determination of tetracyclines. Chemosphere, 338 (2023), Article 139452.
27. S. Zhang, Y.Z. Li, C.L. Fan, J.Q. Liu, Y.Y. Guo, Glutathione-templated blue emitting copper nanoclusters as selective fluorescent probe for quantification of nitrofurazone. Chem. Phys. Lett., 825 (2023), Article 140614.
28. J.M. Xu, X.H. Chen, H.M. Zhou, Y. Zhao, Y.C. Cheng, Y. Wu, J. Zhang, J.Q. Chen, S.J. Zhang, Machine learning-assisted photoluminescent sensor array based on gold nanoclusters for the discrimination of antibiotics with test paper. Talanta, 266 (2024), Article 125122.

29. S.S. Evstigneeva, D.S. Chumakov, R.S. Tumskiy, B.N. Khlebtsov, N.G. Khlebtsov, Detection and imaging of bacterial biofilms with glutathione-stabilized gold nanoclusters. Talanta, 264 (2023), Article 124773.
30. A.H. Hu, Q.X. Duan, X.Y. Xiong, Z. Kang, A.M. Bai, M.M. Yin, Y.J. Hu, Revealing the effects of ligands of silver nanoclusters on the interactions between them and ctDNA: Abstraction to visualization. Int. J. Biol. Macromol., 236 (2023), Article 123965.
31. X.X. Wang, Y.H. Bai, X.J. Du, J.L. Han, Y.P. Yang, Theoretical study of construction of medium-sized gold nanoclusters. Chem. Phys. Lett., 830 (2023), Article 140792.
32. R. Nakum, Y. Upadhyay, S.K. Sahoo, Tuning Zn(II) selectivity by conjugating vitamin B6 cofactors over bovine serum albumin stabilized red-emitting silver nanoclusters. Anal. Chim. Acta, 1235 (2022), Article 340538.
33. T. Sasikumar, M. Ilanchelian, Facile preparation of dihydrolipoic acid-stabilized red-emitting silver nanoclusters as a sensitive fluorometric probe for sulfide ions detection. Spectrochim. Acta A, 302 (2023), Article 123034.
34. Z.F. Cai, L.L. Wu, J.R. Xi, E.X. Hao, K.F. Qi, Green and facile synthesis of polyethyleneimine-protected fluorescent silver nanoclusters for the highly specific biosensing of curcumin. Colloid. Surf. A, 615 (2021), Article 126228.
35. S. Swathy, Goldamol S. Pallam, K. Girish Kumar, Tryptophan capped gold–silver bimetallic nanoclusters-based turn-off fluorescence sensor for the determination of histamine. Talanta 256 (2023), Article 124321.
36. Z. S. Kardar, F. Shemirani, R. Zadmard, Determination of iron(II) and iron(III) via static quenching of the fluorescence of tryptophan-protected copper nanoclusters. Microchem. Acta 187 (2020), p. 81.
37. J.B.M. Parambath, S.M. Kanan, A.A. Mohamed, Tryptophan capped gold-aryl nanoparticles for energy transfer study with SARS-CoV-2 spike proteins. Soft Mater. 20 (2022), pp. 405–413.
38. Z. Zaheer, M.A. Malik, F.M. Al-nowaiser, Z. Khan, Preparation of silver nanoparticles using tryptophan and its formation mechanism. Colloids Surf., B, 81 (2010), pp. 587–592.
39. S. Li, G. Li, H. Shi, M. Yang, W. Tan, H. Wang, W. Yang, A fluorescent probe based on tryptophan-coated silver nanoclusters for copper (II) ions detection and bioimaging in cells. Microchem. J. 175 (2022), Article 107222.
40. S. M. Saleh, W. A. El-Sayed, M. A. El-Manawaty, M. Gassoumi, R. Ali, Microwave-Assisted Rapid Synthesis of Luminescent Tryptophan-Stabilized Silver Nanoclusters for Ultra-Sensitive Detection of Fe(III), and Their Application in a Test Strip. Biosensors 12(2022), p. 425.
41. T.U.B. Rao, T. Pradeep, Luminescent Ag7 and Ag8 clusters by interfacial synthesis. Angew. Chem. Int. Ed., 49 (2010), pp. 3925–3929.
42. T.U.B. Rao, B. Nataraju, T. Pradeep, Ag9 quantum cluster through a solid-state route. J. Am. Chem. Soc., 132 (2010), pp. 16304–16307.
43. A.M. Mahmoud, M.H. Mahnashi, K. Alhazzani, A.Z. Alanazi, M.M. Algahtani, A. Alaseem, B.A. Alyami, A.O. AlQarni, M.M. El-Wekil, Nitrogen doped graphene quantum dots based on host guest interaction for selective dual readout of dopamine. Spectrochim. Acta A Mol. Biomol. Spectrosc., 252 (2021), Article 119516.
44. A.O. Alqarni, S.A. Alkahtani, A.M. Mahmoud, M.M. El-Wekil, Design of "Turn On" fluorometric nanoprobe based on nitrogen doped graphene quantum dots modified with β-cyclodextrin and vitamin B6 cofactor for selective sensing of dopamine in human serum. Spectrochim. Acta A Mol. Biomol. Spectr., 248 (2021), Article 119180.
45. C.N. Iswarya, S.C.G.K. Daniel, M. Sivakumar, Studies on L -histidine capped Ag and Au nanoparticles for dopamine detection. Mater. Sci. Eng. C, 75 (2017), pp. 393–401.
46. A. M. Mahmoud, S. S. Abu-Alrub, A. O. Al-Qarni, B. A. Alyami, M. M. El-Wekil, M. Oraby, First report for fluorometric determination of kasugamycin based on amino acid-functionalized bimetallic nanoclusters. Microchem. J. 199 (2024), Article 110012.
47. .M. Guo, W. Zhao, Hydrothermal synthesis of highly fluorescent nitrogen-doped carbon quantum dots with good biocompatibility and the application for sensing ellagic acid. Spectrochim. Acta A, 240 (2020), Article 118580.
48. M.J. Wang, X.B. Zhou, X.Y. Wang, M.K. Wang, X.G. Su, One-step fabrication of wavelength-tunable luminescence of gold-silver bimetallic nanoclusters: robust performance for α-glucosidase assay. Sens. Actuat. B, 345 (2021), Article 130407.
49. Z. Cai, C. Deng, J. Wang, Y. Zuo, J. Wu, X. Wang, T. Lv, Y. Wang, D. Feng, J. Zhao, C. Zhang, J. Zhang, Sensitive and selective determination of aloin with highly stable histidine-capped silver nanoclusters based on the inner filter effect. Colloids and Surfaces A: Physicochemical and Engineering Aspects Volume 627, 20 October 2021, 127224.
50. B. Yan Zhang a, Mei Lv a, Pengfei Gao a, Guomei Zhang a, Lihong Shi a, Mingjian Yuan b, Shaomin Shuang. The synthesis of high bright silver nanoclusters with aggregation-induced emission for detection of tetracycline. Sensors and Actuators B: Chemical Volume 326, 1 January 2021, 129009.
51. M.M. Zhang, X.Y. Dong, Z.Y. Wang, H.Y. Li, S.J. Li, X. Zhao, S.-Q. Zang, AIE triggers the circularly polarized luminescence of atomically precise enantiomeric copper(I) alkynyl clusters. Angew. Chem. Int. Edit., 59 (25) (2020), pp. 10052–10058.
52. Y. Yang, Y. Sun, S. Liao, Z. Wu, R. Yu, Bimetallic gold–silver nanocluster fluorescent probes for Cr(III) and Cr(VI). Anal. Methods, 8 (2016), pp. 7237–7241.
53. Y. S. Alqahtani, A. M. Mahmoud, H. Ibrahim, M. M. El-Wekil, Enhanced fluorescent detection of oxaliplatin via BSA@copper nanoclusters: a targeted approach for cancer drug monitoring. Anal. Methods 16 (2024), pp.3125–3130.
54. Y. Zhang, X. Zhang, H. Xu, S. Zhao, Z. Yang, Z. Pi, X. Yang, X. Liao. A Ratiometric fluorescence probe based on silver nanoclusters and CdSe/ZnS quantum dots for the detection of hydrogen peroxide by aggregation and etching. J. Fluoresc. (2024). https://doi.org/10.1007/s10895-024-03774-x.
55. S. K. Menon, B. R. Mistry, K. V. Joshi, P. G. Sutariya, R. V. Patel, Analytical detection and method development of anticancer drug gemcitabine HCl using gold nanoparticles. Spectrochim. Acta Part A: Mol. Biomol. Spectr. 94 (2012), pp. 235–242.
56. B. Yılmaz, Y. Kadıoğlu, Comparison of zero- and second-order derivative spectrophotometric and HPLC methods for the determination of gemcitabine in human plasma. Il Farmaco 59 (2004), pp. 425–429.
57. K. M. Naik, S.T. Nandibewoor, Electro-oxidation and determination of gemcitabine hydrochloride, an anticancer drug at gold electrode. J. Indust. Engin. Chem. 19 (2013), pp. 1933–1938.
58. G. A. Tığ, B. Zeybek, Ş. Pekyardımcı, Electrochemical DNA biosensor based on poly(2,6-pyridinedicarboxylic acid) modified glassy carbon electrode for the determination of anticancer drug gemcitabine. Talanta 154 (2016), pp. 312–321.
59. Z. Shekarbeygi, C. Karami, E. Esmaeili, S. Moradi, M. Shahlaei, Development of Ag nanoparticle-carbon quantum dot nanocomplex as fluorescence sensor for determination of gemcitabine. Spectrochim. Acta A, 262 (2021), Article 120148.
60. S. Najafi, S. Amani, M. Shahlaei, Rapid determination of the anticancer agent Gemcitabine in biological samples by fluorescence sensor based on Au-doped CdTe. J. Mol. Liq. 266 (2018), pp. 514–521.

61. Lafazanis, E. Begas, I. Papapostolou, H. Iatrou, N Sakellaridis, D. Vlassopoulos, K. Dimas, K. Dimas, development and validation of a simple and reliable HPLC-UV method for determining gemcitabine levels: application in pharmacokinetic analysis. Medicina 2024, 60(6), 864.
62. B.J. Muller-Borer, M.C. Collins, P.R. Gunst, W.E. Cascio, A.P. Kypson, Quantum dot labeling of mesenchymal stem cells. J. Nanobiotechnol., 5 (2007), pp. 3071–3079.
63. Y. S. Alqahtani, A. M. Mahmoud, A. B. H. Ali, M. M El-Wekil, Enhanced fluorometric detection of histamine using red emissive amino acid-functionalized bimetallic nanoclusters. RSC Adv.14 (2024), pp. 18970–18977.
64. P.C. Wu, C.Y. Chen, C.W. Chang, The fluorescence quenching and aggregation induced emission behaviour of silver nanoclusters labelled on poly (acrylic acid- co -maleic acid). New J. Chem., 42 (2018), pp. 3459–3464.
65. U. Sivasankaran, S. Jesny, A.R. Jose, K. Girish Kumar, Fluorescence determination of glutathione using tissue paper-derived carbon dots as fluorophores, Anal. Sci. 33(2017), pp. 281–285.
66. M. H. Mahnashi, A. M. Mahmoud, M. M. El-Wekil, R. Y. Shahin, An innovative enzyme-free ratiometric determination of uric acid based on polyethyleneimine modified graphene quantum dots pretreated with periodate combined with eosin Y. Microchem. J. 193 (2023), p.109062.
67. B. A. Alyami, A. M. Mahmoud, A. O. Alqarni, M. M. El-Wekil, Intrinsic self-calibration electrostatic-controlled ratiometric fluorescence assay of histamine in human serum and canned tuna fish samples. Microchem. J. 195 (2023), p.1 109388.
68. Y.J. Hu, H.G. Yu, J.X. Dong, X. Yang, Y. Liu, Spectroscopic studies on the interaction between 3,4,5-trimethoxybenzoic acid and bovine serum albumin Spectrochim. Acta A Mol. Biomol. Spectrosc., 65 (2006), pp. 988–992.
69. S. Moradi, M. Taran, M. Shahlaei, Investigation on human serum albumin and Gum Tragacanth interactions using experimental and computational methods. Int. J. Biol. Macromol., 107 (2018), pp. 2525–2533.
70. P.N. Naik, S.A. Chimatadar, S.T. Nandibewoor, Interaction between a potent corticosteroid drug - dexamethasone with bovine serum albumin and human serum albumin: a fluorescence quenching and fourier transformation infrared spectroscopy study. J. Photochem. Photobiol. B Biol., 100 (2010), pp. 147–159.